J Mater Sci: Mater Med (2010) 21:2453–2462
DOI 10.1007/s10856-010-4101-x

Determination of antibacterial properties and cytocompatibility of silver-loaded coral hydroxyapatite

Yu Zhang · Qing-Shui Yin · Yu Zhang · Hong Xia · Fu-Zhi Ai · Yan-Peng Jiao · Xu-Qiong Chen

Received: 28 November 2009 / Accepted: 20 May 2010 / Published online: 5 June 2010

Abstract In this study, silver-loaded coral hydroxyapatites (SLCHAs) were used as scaffolds for bone tissue engineering. The SLCHAs were prepared by surface adsorption process and ion-exchange reaction between Ca^{2+} of coral hydroxyapatite (CHA) and Ag^{+} of silver nitrate with different concentrations at room temperature. The properties of the composite SLCHAs were investigated by inductively coupled plasma-atomic emission spectrometry (ICP-AES), scanning electron microscropy (SEM) equipped with backscattered electron detector (BSE), and energy-dispersive X-ray spectrometer (EDS). The SEM images showed that the morphology of the SLCHAs depended on the content of Ag^{+}, and the silver ions were uniformly distributed on the surface of SLCHAs. The ICP-AES results demonstrated that the silver content of the SLCHAs decreased along with the decrease of the concentration of silver nitrate. The SLCHAs were found effective against *Escherichia coli* and *Staphylococcus aureus* by antibacterial test. Mouse embryonic pre-osteoblast cells (MC3T3-E1) were used to test the cytocompatibility of SLCHAs, CHA, and pure coral. Cell morphology and cell proliferation were studied with SEM, laser scanning confocal microscope (LSCM), and MTT (3-(4, 5-dimethylthiazol-2-yl)-2,5-diphenyl tetrazolium bromide) assay after 1, 3, and 5 days of culture. The results indicated the cell morphology and proliferation on the scaffolds of Ag^{+} (13.6 μg/ml)/CHA and Ag^{+} (1.7 μg/ml)/CHA were better than that on Ag^{+} (170 μg/ml)/CHA. In addition, adhesion of MC3T3-E1 on the scaffolds showed that the confluent cells showed fusiform shape and arranged tightly on the scaffolds. All the results showed that the antibacterial SLCHAs would have potential clinical application as the scaffolds for bone tissue engineering.

Y. Zhang (✉) · Q.-S. Yin · Y. Zhang · H. Xia · F.-Z. Ai · X.-Q. Chen
Department of Orthopaedics, Guangzhou General Hospital of Guangzhou Military Command, Guangzhou 510010, People's Republic of China
e-mail: zhangyu1980cmu@yahoo.com.cn

Y. Zhang
Graduate School of Southern Medical University (First Military Medical University), Guangzhou 510515, People's Republic of China

Y.-P. Jiao
Department of Materials Science and Engineering, Jinan University, Guangzhou 510630, People's Republic of China

1 Introduction

The regeneration potential of human bone is limited in the cases of repair of large bone defects, such as those associated with comminuted fractures or bone tumor resections. At recent times, because of more and more traffic accidents, earthquakes and wars, bacterial infections often result from heavy contamination of the wound with soil, organic material, etc. Despite repetitive and aggressive debridement, a large number of fractures still remain contaminated and become infected, which limits one-stage bone grafting [1–3].

At present, local antibiotic therapy has been considered as a safe technique resulting in high local concentration of antibiotics with minimal systemic levels [4–6]. However, the nature of infectious processes has been greatly changed with the introduction of mutated forms antibiotic-resistant to the action of most antibiotics. As a result, the effective treatment of local infections has become much more difficult in requiring systemic or localized administration of large doses of multiple antibiotics, which often has attendant undesirable side effects and clinical limitations [7, 8].

Because infections occur when bacterial numbers overwhelm local defenses, healing is promoted by reducing the numbers of bacteria in the wound to a level that can be eliminated by local defenses. Rapid and efficient wound healing will reduce the cost of treatment and promote an earlier return to function.

Therefore, the synthetic bone grafts, such as hydroxyapatites (HA), cements and different types of polymers and composites, have been widely developed to replace autografts and allografts [9–12]. CHA has been widely used as scaffolds in various biomedical applications [13–16] due to its biodegradability, biocompatibility, non-toxicity, good mechanical properties, bioconductivity, and 3D sponge-like porous structure. However, the incidence of biomaterial-centered infection, often leading to revision surgery, underlies the need to improve the properties of existing biomaterials.

An easily achieved approach to increasing the antimicrobial property of the scaffold is to incorporate an antibacterial agent into the bone graft. It has long been known that the antimicrobial properties of the silver ion have been exploited since ancient times by Mediterranean and Asiatic cultures. The historic use of silver in surgical treatment of wounds and broken bones is well documented [17–19]. The significant feature of silver ion is its broad-spectrum bactericidal property [20–22] for Gram-negative and Gram-positive pathogens, which is particularly significant for polymicrobial colonization associated with biomaterials-related infections. It is generally found that bacteria show a low propensity to develop resistance to silver-based products, and therefore both metallic and ionic silver have been incorporated into several biomaterials such as polyurethane, hydroxyapatite and bioactive glasses [23–25]. In addition, silver-based vascular and urinary catheters have been in clinical use [26]. Therefore, it would be interesting to incorporate ionic silver in CHA to increase its bactericidal property. At present, many studies have attempted to investigate the possible use of SLCHAs as antibacterial bone grafts. However, there is little report about the relationship between silver content and cytocompatibility. In particular, the effectiveness of SLCHAs occurs because of the slow release of silver ions, resulting in continuing bactericidal concentrations of silver in the Luria–Bertani Broth (LB) agar plate.

In this study, composite antimicrobial scaffolds were obtained by soaking CHA in silver nitrate solution. Silver content in the CHA composite was test quantitatively by inductively coupled plasma-atomic emission spectrometry (ICP-AES). The morphology and surface composition of the SLCHAs were studied by scanning electron microscopy (SEM) coupled with backscattered electron detector (BSE) and energy dispersive X-ray spectroscopy (EDS). The cytocompatibility of SLCHAs, CHA and pure coral, such as cell morphology and cell proliferation, was investigated with SEM, laser scanning confocal microscopy (LSCM) and MTT (3-(4,5-dimethylthiazol-2-yl)-2,5-diphenyl tetrazolium bromide) assay. Furthermore, bactericidal property was evaluated by using a modified Kirby–Bauer technique.

2 Materials and methods

2.1 Materials

CHA was provided by Guangdong Key Laboratory of Orthopaedic Technology and Implant Materials in China. CHA was cut into cuboidal samples ($\sim 132.51 \pm 29.12$ mg) with a dimension of 5 mm × 5 mm × 5 mm in size. Silver nitrate (Molecular Weight = 169.87) was purchased from Sigma. All reagents were analytical grade and used without further purification.

2.2 Sample preparation

To introduce silver ions through the ion-exchange process, SLCHAs were obtained by socking CHA in silver nitrate ($AgNO_3$, Sigma) solutions (pH = 5.8) containing different concentrations of silver ions (1.7, 8.5, 13.6, 17, 85, 170, and 1700 μg/ml, respectively) at room temperature for 24 h. Then the samples were removed and carefully rinsed with distilled water several times, and frozen overnight in a vacuum freeze-dryer (LGJ-12, Beijing, China).

2.3 Characterization of SLCHA scaffolds

The total silver content in the SLCHAs was determined by X Series ICP-AES (Thermo Fisher Scientific, USA). The morphology and surface composition of the SLCHAs were studied by using SEM (Quanta-400, Fei, Netherlands) equipped with a BSE (HKL, Oxford, UK) and an EDS (INCA, Oxford, UK). CHA samples were used as control.

2.4 Antibacterial property

Escherichia coli (*E. coli,* ATCC25922) and *Staphylococcus aureus* (*S. aureus*, ATCC 25923) were incubated in sterilized LB broth and then cultivated overnight at 37°C in a shaking incubator. The disc diffusion method was carried out in LB agar plate using a modified Kirby–Bauer technique. The bacterial suspension used for the tests (100 μl of 10^5, 10^6 colony forming units, CFU) was uniformly dispersed on the surface of a LB agar plate before placing the test samples on it. Then the agar plates containing the test samples or control were incubated at 37°C for 24 h and the inhibition zones surrounding the sample were measured. CHA samples and 15 μl Ampicillin (Amp, Shanghai,

China) with the concentration of 50 μg/ml were used as control.

2.5 Cell cultures

The cytocompatibility of the SLCHAs, CHA and pure coral was investigated with the MC3T3-E1 pre-osteoblastic cells according to the protocol reported previously [27]. The cells were cultured at 37°C in a humidified atmosphere of 5% CO_2 in air, in 25-cm^2 tissue culture flasks. The cell culture medium used was modified Eagle's minimum essential medium (α-MEM, Hyclone, USA) with 4.5 g/l glucose, 10% fetal calf serum (Hyclone), 10 μg/ml ascorbic acid, 50 U/ml penicillin, and 50 U/ml streptomycin.

The cells with a density of about 10^4 cells/cm^2 were suspended in culture medium, dispersed over the composite scaffolds, which were sterilized by ^{60}Co γ-irradiation at a dose of 25 kGy, in a 48-well plate for MTT assay, SEM observation and LSCM (OLYMPUS FluoView™ FV1000, Olympus, Japan). The assays were performed at 1, 3, and 5 days, respectively.

2.6 Cell morphology

After 1, 3 and 5 days of culture, the SLCHAs, CHA, and pure coral were washed with PBS to eliminate non-adherent cells and then fixed with 2.5% glutaraldehyde for 20 min at room temperature, dehydrated through a series of graded alcohol solutions, and then freeze-dried overnight. All samples were sputter coated with gold before SEM examination. Cells cultured on the scaffolds were also observed with LSCM after being washed with PBS twice and the cell nuclei were colored with propidium iodide (PI, Sigma, St.Louis, MO, USA) to visualize the cells. Cells were incubated in 5 μg/ml PI solution diluted with PBS buffer for 30 min at 37°C. Then the samples were washed with PBS three times. The mixture of 50% glycerin and 50% PBS was added to keep the samples wet during the examination period. According to the emission wavelength of PI, the filter was set 570 LP and the laser was 543 nm in the fluorescence mode. In the reflection mode, the laser was 488 nm and the filter was set 488/4 nm.

2.7 MTT assay

The MTT (Sigma, St. Louis, MO, USA) assay [28] was used to evaluate the level of cellular energy metabolism and indirectly indicate the condition of cell proliferation. After MC3T3-E1 pre-osteoblastic cells were incubated in 48-well plate for 1, 3 and 5 days, the cell proliferation was determined by MTT assay. Three samples per group were evaluated. MTT solution at 5 mg/ml was prepared by dissolving MTT in PBS which was then filter-sterilized, which was added to each well and cultured at 37°C for 4 h in humidified atmosphere of 5% CO_2 in air. At the end of the assay, the blue formazan reaction product was dissolved by adding 400 μl dimethyl sulfoxide (DMSO, Sigma) and 150 μl of the solution was then transferred to a 96-well tissue culture plate. DMSO (400 μl) and pure coral were used as blank control group. Optical density of the solution in each well was measured at a wavelength of 490 nm using a Microplate reader (Biocell-2010, Austria). The absorbance at 490 nm can be used to analyze the cell growing activity. Data are presented as mean with standard deviation.

2.8 Statistics

The quantitative data are presented as mean and standard deviation. The statistical significance of the differences among the experimental groups was evaluated by univariate ANOVA and LSD with the SPSS13.0. Value $P \leq 0.05$ was considered significant.

3 Results and discussion

3.1 Characterization of SLCHA samples

3.1.1 Measurement of total silver content

Fig. 1 illustrates the total silver content of different SLCHA samples. The silver content of the SLCHA samples in different groups is 167.90 ± 11.00 μg/g, 83.42 ± 4.51 μg/g, 30.20 ± 2.32 μg/g, 22.39 ± 4.09 μg/g, and 15.11 ± 0.55 μg/g, respectively. It indicates that the silver content of the SLCHAs measured decreases along with the decrease of the concentration of silver nitrate. Meanwhile, according to

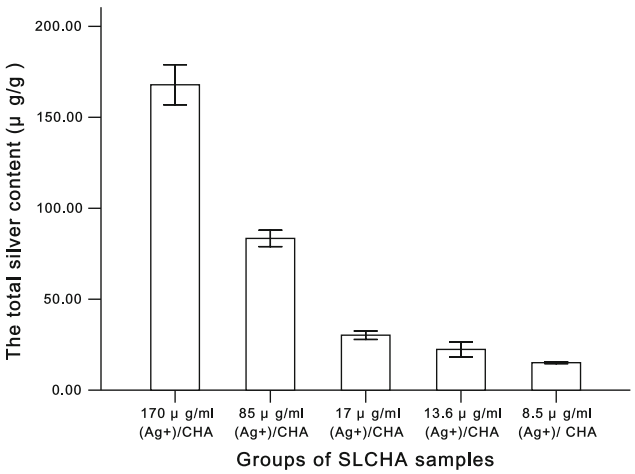

Fig. 1 The total silver content of different SLCHA samples (C Value, $n = 3$)

these results, silver content in scaffolds depended on the ionic concentration of solution. As reported [29, 30], the ion-exchange reactions between Ag^{+} and Ca^{2+} were also influenced by multiple factors such as pH value of solution, reaction time, ion competition, etc. We are far from trying to extrapolate the results to the whole preparation, especially considering that the set of SLCHA are not typical of those currently being prepared. Even so, it could be important to review the subject, considering the increasing production of SLCHA scaffolds.

3.1.2 *Morphology and surface composition of the SLCHAs*

Fig. 2A and B present eight SEM images, taken with related EDS spectra. Fig. 2A (a–g) are images from the surface of the SLCHA sample, respectively, which

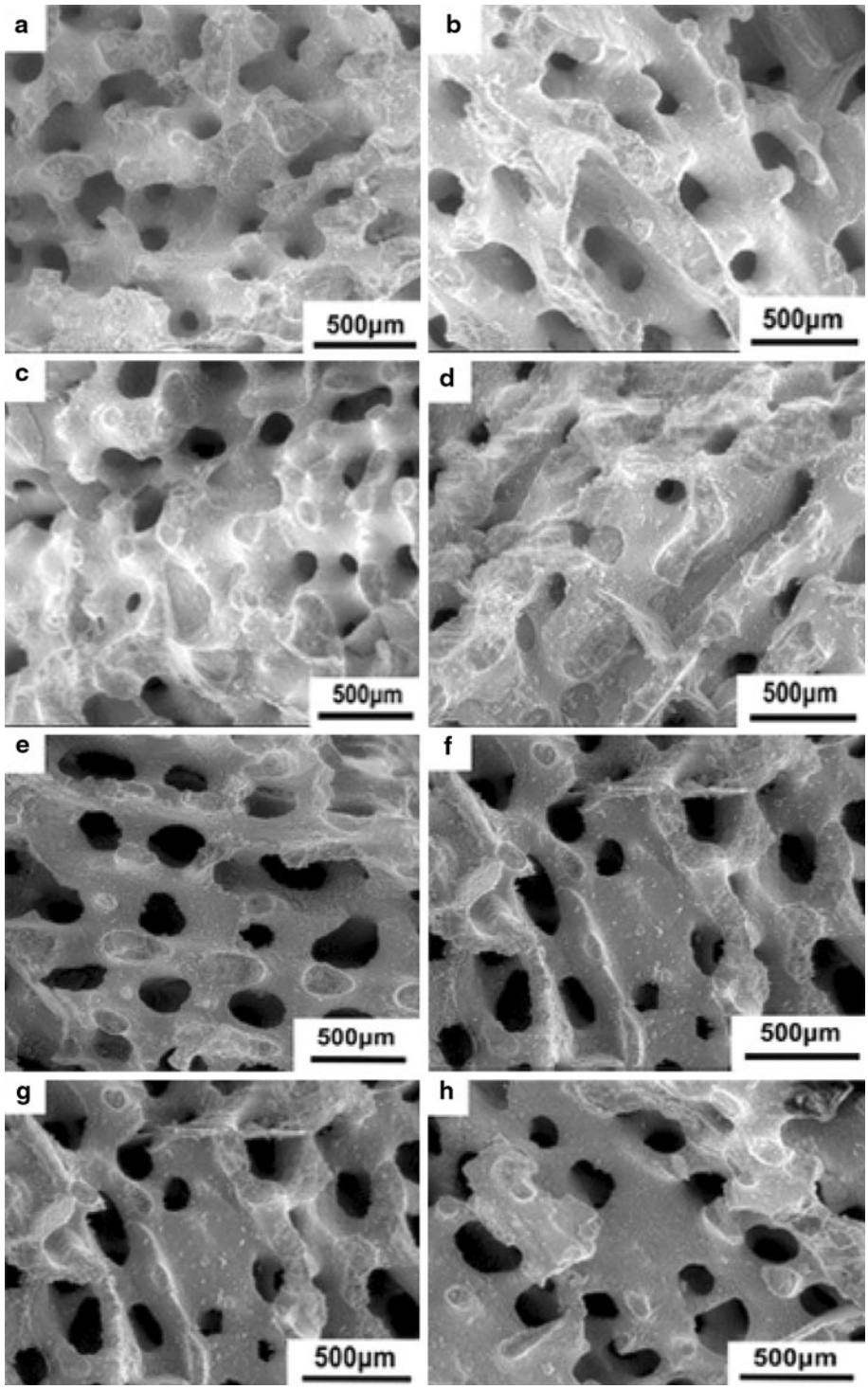

Fig. 2 SEM images with EDS **A** and BSE micrographs of SLCHA samples **B,** and CHA **C**: **a**, 1700 μg/ml (Ag^{+})/CHA; **b**, 170 μg/ml (Ag^{+})/CHA; **c**, 85 μg/ml (Ag^{+})/CHA; **d**, 17 μg/ml (Ag^{+})/CHA; **e**, 13.6 μg/ml (Ag^{+})/CHA; **f**, 8.5 μg/ml (Ag^{+})/CHA; **g**, 1.7 μg/ml (Ag^{+})/CHA; and **h**, CHA. No apparent differences in porous structure among the SLCHA samples and CHA could be seen in the Fig. 2**A**. The tables standing for the composition of inner middle portion of SLCHA samples and CHA were exhibited in Fig. 2**B**. The bright spots for tiny particles with the heavy silver atoms were marked with black arrows over the darker background of the scaffold in Fig. 2**C**

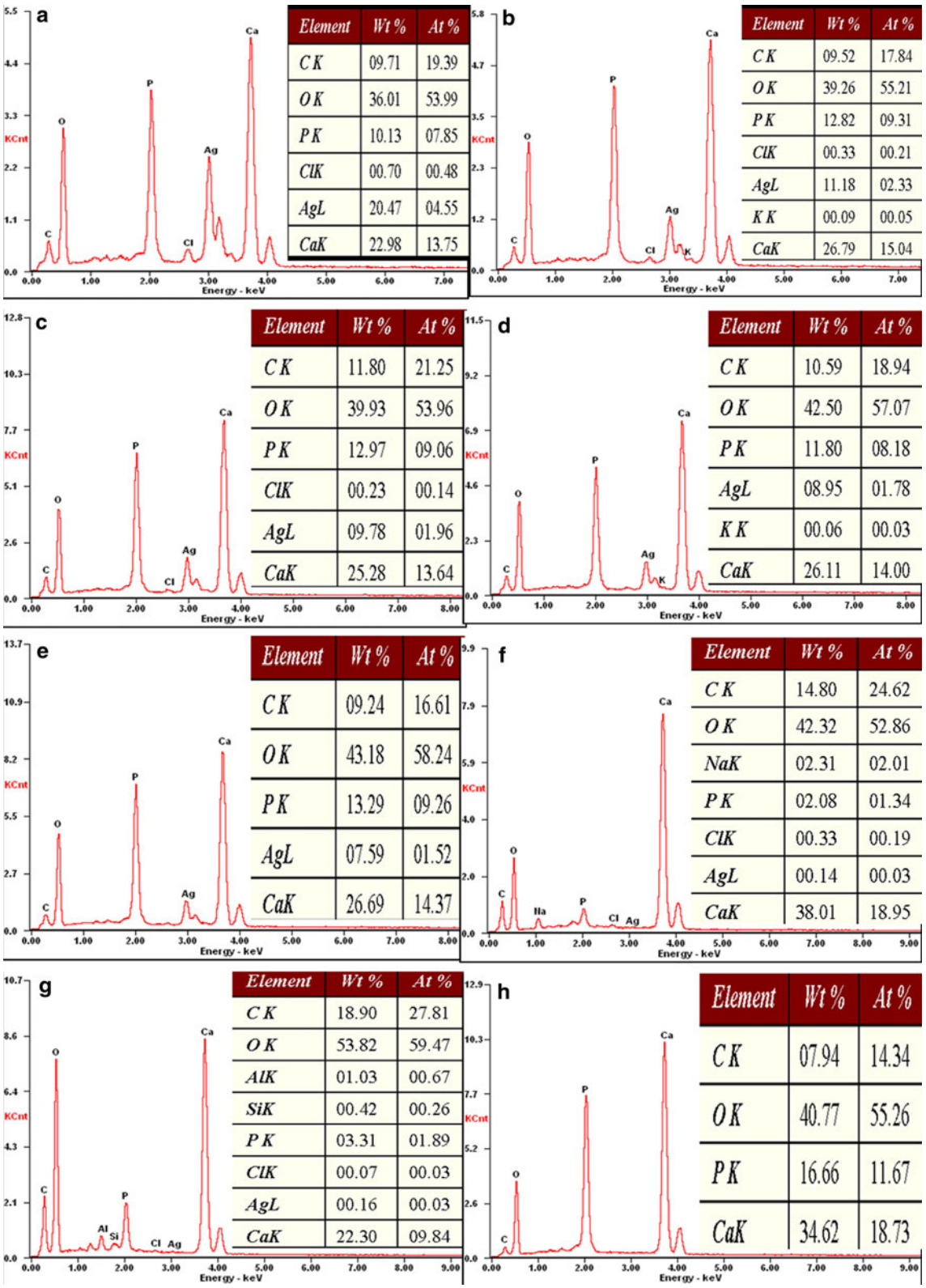

Fig. 2 continued

indicate that the SLCHA product still maintained the porous structure of the original coral. The EDS spectra in Fig. 2B (a–g) from the inner middle portion show characteristic peaks of calcium, carbon, silver, phosphorus, and oxygen, which demonstrate the conversion from Ca-rich CHA to Ag^{+}-CHA through the ion-exchange

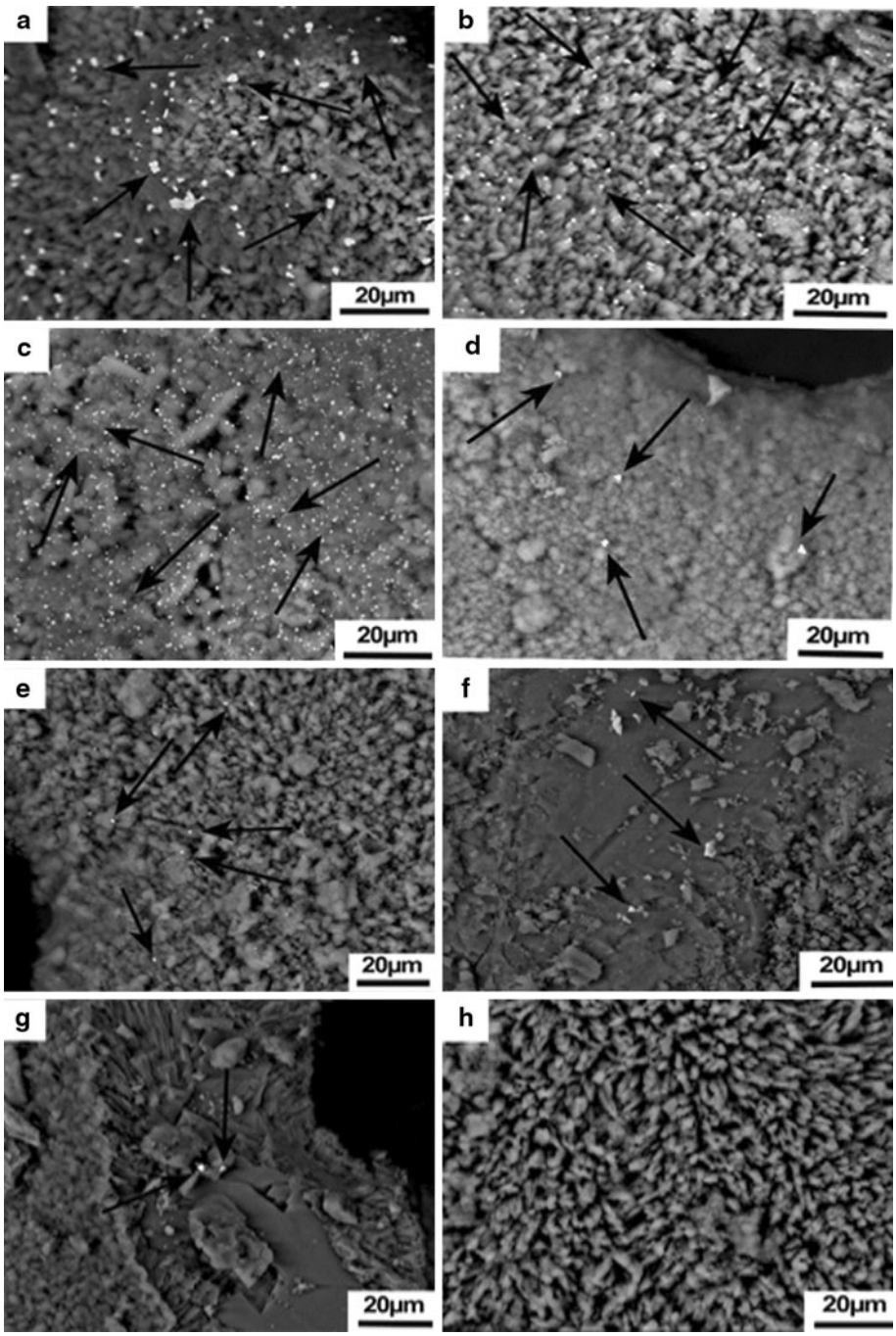

Fig. 2 continued

reaction. The EDS spectrum in Fig. 2B (h) indicates the characteristic peaks of calcium, carbon, phosphorus, and oxygen expected for HA, consistent with previous reports [31, 32]. Some precipitates were also observed by BSE on the struts at the sample surface in Fig. 2C (a–g). These precipitates are believed to be AgCl, formed through the dissolution–reprecipitation process during conversion course. The AgCl precipitates on the struts make them look thicker than that on the untreated struts in the CHA (Fig. 2C (h)). In addition, Fig. 2C (a–g) demonstrates that the content of precipitates decreases along with the decrease of the concentration of silver nitrate, in accordance with the results of Fig. 1. On the other hand, the fresh CHA surface of a strut (Fig. 2C (h)) consists of large particles with dense structures, which is considered as HA converted from coral. Therefore, the main conversion mechanism in the experiment is the ion-exchange reaction. It is a secondary dissolution–reprecipitation process, during which AgCl precipitates form on the surfaces of the sample.

3.1.3 *In vitro antibacterial effect*

Using a modified Kirby–Bauer assay [33], the bactericidal properties of seven SLCHA samples and pure CHA sample were compared. After 24 h of incubation at 37°C, the SLCHA samples show antibacterial effect on Gram-positive *S. aureus* and Gram-negative *E. coli* in an agar plate besides the lowest silver-loading dosage and the control (shown in Fig. 3). The diameter of the zone of inhibition for the 1700 μg/ml (Ag^+)/CHA is ca. 19 mm, whereas that of 13.6 μg/ml (Ag^+)/CHA is ca. 13 mm (where the size of both blocks is ca. 10 mm). This result indicates that the 1700 μg/ml (Ag^+)/CHA has a more effective contact biocidal property than the 13.6 μg/ml (Ag^+)/CHA. As a control, the pure CHA sample showed no inhibition ability. Elemental silver has been believed to have antimicrobial function either as a release system for silver ions or as a contact-active material [34]. In the present study, the SLCHA samples seem to be not only contact-active but also slow-releasing. The diffusing ability of silver ions on agar plate might be blocked by the formation of secondary compounds such as AgCl in the Kirby–Bauer test media [35], which is the limitation of the Kirby–Bauer technique as a quantitative tool to determine the antimicrobial activity. In the case of SLCHA, the silver can freely diffuse into the test media and act as biocidal agents. In addition, the SLCHA provides high surface area to contact bacteria. Therefore, the SLCHA has a superior contact antibacterial property.

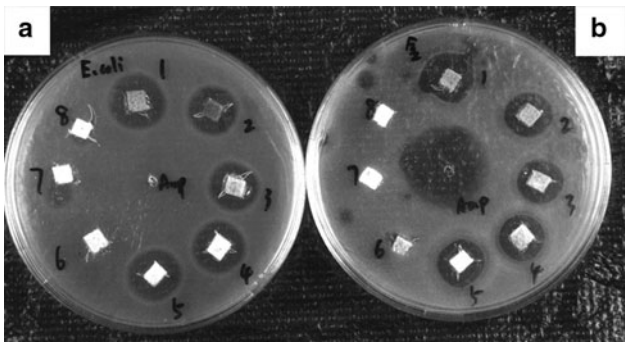

Fig. 3 Antibacterial test results for *E. coli* **a** and *S. aureus* **b** after 24 h incubation: **1** 1700 μg/ml (Ag^+)/CHA, **2** 170 μg/ml (Ag^+)/CHA, **3** 85 μg/ml (Ag^+)/CHA, **4** 17 μg/ml (Ag^+)/CHA, **5** 13.6 μg/ml (Ag^+)/CHA, **6** 8.5 μg/ml (Ag^+)/CHA, **7** 1.7 μg/ml (Ag^+)/CHA, and **8** CHA. Amp with the concentration of 50 μg/ml was used as control

3.1.4 *Cell cultures*

3.1.4.1 Cell distribution and morphology The MC3T3-E1 cells were seeded in the three-dimensional scaffolds and

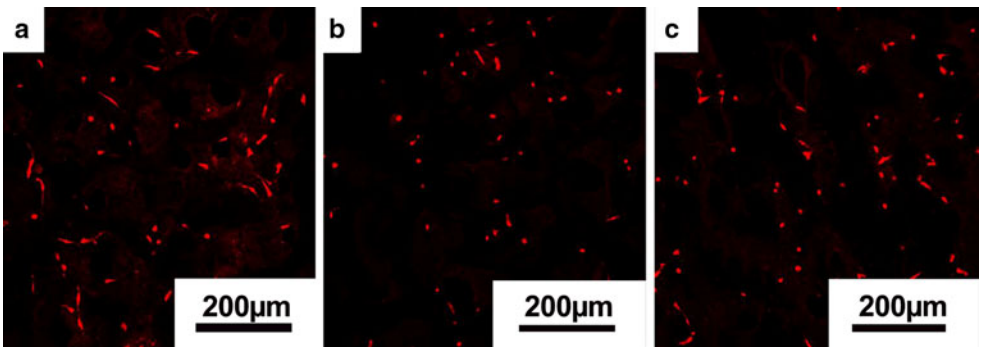

Fig. 4 Fluorescence microscopy images of MC3T3-E1 cells cultured in different scaffolds for 2 days: **a,** silver ion (13.6 μg/ml)/CHA; **b,** CHA; and **c,** pure coral. The bright red signals stand for cell nuclei

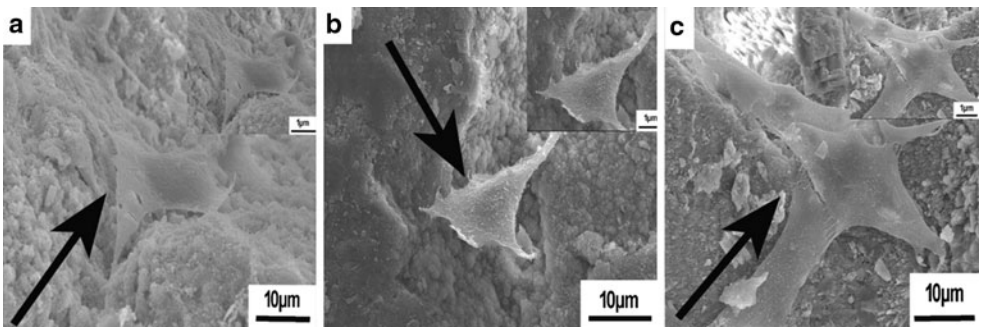

Fig. 5 SEM images of MC3T3-E1 cells cultured in different scaffolds for 2 days: **a,** silver ion (13.6 μg/ml)/CHA; **b,** CHA; and **c,** pure coral. Cells were marked with black arrows

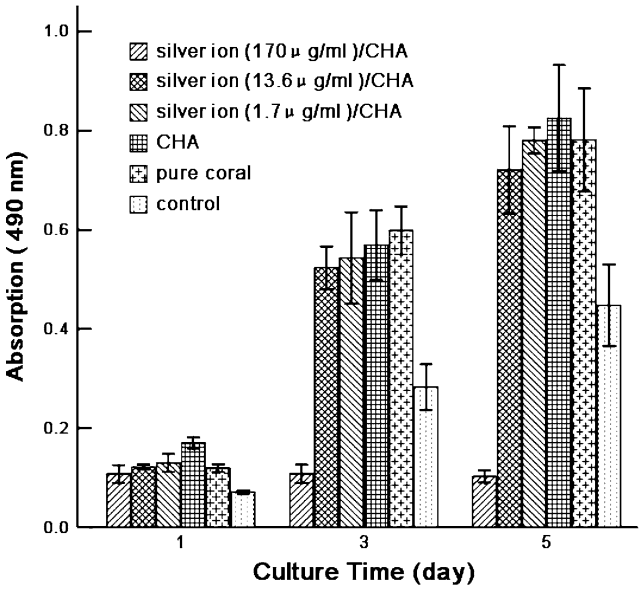

Fig. 6 MTT assay of cell viability of MC3T3-E1 cells cultured in scaffolds. Proliferation of MC3T3-E1 cells is not significantly different from that on CHA, pure coral, and the lower silver concentrations ($P = 0.538, 0.076, 0.298, 0.216, 0.658, 0.411$) at days 1, 3, and 5, but is significantly higher on the control group and 170 μg/ml Ag^+/CHA group ($P = 0.000$). Compared to blank control group, the proliferation of the cells cultured in each scaffold increased with the increasing of culture time besides the CHA soaked with 170 μg/ml Ag^+ ions

cultured for 2 days. The cell morphology and uniform distribution in the scaffolds observed by LSCM and SEM can be seen in Fig. 4 and Fig. 5, respectively. LSCM images of MC3T3-E1 cells (Fig. 4a–c) demonstrated that most of the cells were polygonal in shape, fully spread. The amount of MC3T3-E1 cells attached to the scaffolds was indistinguishable, which indicated that the SLCHA sample in this group (Fig. 4a) had good biocompatibility in 3D space. Furthermore, the SEM pictures (Fig. 5a–c) showed that the MC3T3-E1 cells reached out ''pseudopods'' and were larger in c than those in a and b in 3D space. But in the composite scaffolds that had silver dosage from zero to 13.6 μg/ml, the ''pseudopods'' was more obvious, progressively. LSCM images implied that the cell distributed evenly with decrease of silver content, but the proliferation of cells is not affected by the smaller silver content.

3.1.5 Cell proliferation in 3D scaffolds

MTT assay was used to assess the cell viability and proliferation of MC3T3-E1 cells cultured in different 3D scaffolds with 1, 3, and 5 days of culture, as shown in Fig. 6. The results of the repeated-measures ANOVA and LSD are summarized in Table 1. It can be seen that significant differences exist among the different groups ($F = 76.457$, $P = 0.000$). Proliferation of MC3T3-E1 cells is not significantly different from that on CHA, pure coral, and the lower silver concentrations ($P = 0.538$, 0.076, 0.298, 0.216, 0.658, 0.411) at days 1, 3,and 5 (Fig. 6), but is significantly higher on the control group and 170 μg/ml Ag^+/CHA group ($P = 0.000$). Compared to blank control group, the proliferation of the cells cultured in each scaffold increased with the increasing of culture time besides

Table 1 The effect of different bone substitutes on MTT assay of MC3T3-E1 cell for 1, 3, and 5 d. ($\bar{x} \pm$ SD, OD Value, n = 3)

Groups		Cultural time			Sum	*F*	*P*
		1 d	3 d	5 d			
170 μg/ml Ag^+/CHA	$\bar{x}$	0.1077	0.1080	0.1027	0.1061	0.099	0.907
	s	0.0180	0.0182	0.0127	0.0145		
13.6 μg/ml Ag^+/CHA	$\bar{x}$	0.1217	0.5233	0.7207	0.4552	88.183	0.000
	s	0.0049	0.0429	0.0875	0.2688		
1.7 μg/ml Ag^+/CHA	$\bar{x}$	0.1297	0.5430	0.7800	0.4842	102.147	0.001
	s	0.0180	0.0924	0.0261	0.2892		
CHA	$\bar{x}$	0.1700	0.5687	0.8250	0.5212	59.365	0.000
	s	0.0110	0.0704	0.1069	0.2930		
Pure coral	$\bar{x}$	0.1193	0.5987	0.7810	0.4997	79.333	0.000
	s	0.0078	0.0485	0.1041	0.3015		
Control	$\bar{x}$	0.0713	0.2827	0.4477	0.2672	36.144	0.000
	s	0.0032	0.0459	0.0821	0.1700		
Sum	$\bar{x}$	0.1199	0.4374	0.6095	0.3889	341.615*	0.000*
	s	0.0317	0.1914	0.2740	0.2794		
F		21.355	34.725	38.436	76.457*	($F = 17.131$, $P = 0.000$)#	
P		0.000	0.000	0.000	0.000*		

* *F* statistic and *P* value of main effect; # *F* statistic and *P* value of crossover effect

the CHA soaked with 170 μg/ml Ag^+ ions. In this study, the proliferation of the cells cultured in samples with lower silver-ionic content was similar to that in CHA and that in pure coral scaffold. In addition, the proliferation of MC3T3-E1 cells was improved with different concentration of silver ion. In Fig. 6, the cell proliferation and growth were best in CHA scaffold at day 5. The absorbance at 490 nm was almost 0.83, which was 4.85 times higher than that in day 1.

4 Conclusions

In this study, silver ions were successfully introduced to the CHA scaffolds by ion-exchange reaction and precipitation process to improve its antibacterial property of CHA scaffolds. In addition, the scaffolds obtained by soaking with appropriate concentration of silver-ion solution was beneficial to keep the MC3T3-E1 compatibility of CHA substrates, and MC3T3-E1 cell growth may be affected by the silver ion content. Importantly, the composite SLCHA scaffolds had an excellent biocidal potential against Gram-positive bacteria (*S. aureus*) as well as Gram-negative bacteria (*E. coli*). According to these results, it is anticipated that this SLCHA scaffold can be potentially used in various clinical applications in bone tissue engineering.

Acknowledgements This work was financially supported by a grant from the program for Science and Technology Key of Guangdong Province (2003C104004 and 2004B33101005) and eleventh five-year plan of military (06G045) in China through the Guangdong Key Laboratory of Orthopaedic Technology and Implant Materials in China.

References

1. Winkler H, Kaudela K, Stoiber A, Menschik F. Bone grafts impregnated with antibiotics as a tool for treating infected implants in orthopedic surgery – one stage revision results. Cell Tissue Banking. 2006;7:319.
2. Tropet Y, Garbuio P, Obert L, Jeunet L, Elias B. One-stage emergency treatment of open grade IIIb tibial shaft fractures with bone loss. Ann Plast Surg. 2001;46:113.
3. DeCoster TA, Gehlert RJ, Mikola EA, Pirela-Cruz MA. Management of posttraumatic segmental bone defects. J. Am. Acad. Orthop. Surg. 2004;12:28.
4. Zalavras CG, Patzakis MJ, Holtom P. Local antibiotic therapy in the treatment of open fractures and osteomyelitis. Clin. Orthop. Relat. Res. 2004;427:86.
5. Garvin K, Feschuk C. Polylactide-polyglycolide antibiotic implants. Clin. Orthop. Relat. Res. 2005;437:105.
6. Branstetter JG, Jackson SR, Haggard WO, Richelsoph KC, Wenke JC. Locally-administered antibiotics in wounds in a limb. J Bone Joint Surg Br. 2009;91:1106.
7. Gemmell CG, Edwards DI, Fraise AP, Gould FK, Ridgway GL, Warren RE. Guidelines for the prophylaxis and treatment of methicillin-resistant Staphylococcus aureus (MRSA) infections in the UK. J Antimicrob Chemother. 2006;57:589.
8. Couce A, Blázquez J. Side effects of antibiotics on genetic variability. FEMS Microbiol Rev. 2009;33:531.
9. Karageorgiou V, Kaplan D. Porosity of 3D biomaterials scaffolds and osteogenesis. Biomaterials. 2005;26:5474.
10. Hing KA. Bioceramic bone graft substitutes: influence of porosity and chemistry. Int J Appl Ceram Technol. 2005;2:184.
11. LeGeros RZ. Properties of osteoconductive biomaterials: calcium phosphates. Clin Orthop Relat Res. 2002;395:81.
12. Vallet-Regı M, ′Gonza′lez-Calbet JM. Calcium phosphates as substitution of bone tissues prog. Solid State Chem. 2004;32:1.
13. Vacanti CA, Bonassar LJ, Vacanti MP, Shufflebarger J. Replacement of an avulsed phalanx with tissue-engineered bone. N Engl J Med. 2001;344:1511.
14. Damien E, Revell PA. Coralline hydroxyapatite bone graft substitute: a review of experimental studies and biomedical applications. J. Appl. Biomateri. & Biomechan. 2004;2:65.
15. Hsu CJ, Chou WY, Teng HP, Chang WN, Chou YJ. Coralline hydroxyapatite and laminectomy-derived bone as adjuvant graft material for lumbar posterolateral fusion. J. Neurosurg. Spine. 2005;3:271.
16. Wasielewski RC, Sheridan KC, Lubbers MA. Coralline hydroxyapatite in complex acetabular reconstruction. Orthopedics. 2008;31:367.
17. Alexander JW. History of the medical use of silver. Surgical Infections. 2009;10:289.
18. Lo SF, Hayter M, Chang CJ, Hu WY, Lee LL. A systematic review of silver-releasing dressings in the management of infected chronic wounds. J. Clin. Nurs. 2008;17:1973.
19. Huckfeldt R, Redmond C, Mikkelson D, Finley PJ, Lowe C, Robertson J. A clinical trial to investigate the effect of silver nylon dressings on mediastinitis rates in postoperative cardiac sternotomy. Ostomy Wound Management. 2008;54:36.
20. Kim J, Lee CH, Cho M, Yoon J. Enhanced inactivation of E coli and MS2 phage by silver ions combined with UV-A and visible light irradiation. Water Res. 2008;42:356.
21. Feng QL, Wu J, Chen GQ, Cui FZ, Kim TN, Kim JO. A mechanistic study of the antibacterial effect of silver ions on Escherichia coli and Staphylococcus aureus. J Biomed Mater Res. 2000;52:662.
22. Kim J, Lee JH, Hahn JS, Gu MB, Yoon J. Silver-ion-mediated reactive oxygen species generation affecting bactericidal activity. Water Res. 2009;43:1027.
23. Tiller JC, Liao CJ, Lewis K, Klibanov AM. Designing surfaces that kill bacteria on contact. Proc Natl Acad Sci USA. 2001;98:5981.
24. Bosetti M, Masse A, Tobin E, Cannas M. Silver coated materials for external fixation devices: in vitro biocompatibility and genotoxicity. Biomaterials. 2002;23:887.
25. Blaker JJ, Boccaccini AR, Nazhat SN. Thermal characterizations of silver-containing bioactive glass-coated sutures. J Biomater Appl. 2005;20:81.
26. Silver S, Phung LT, Silver G. Silver as biocides in burn and wound dressings and bacterial resistance to silver compounds. J Ind Microbiol Biotechnol. 2006;33:627.
27. Manjubala I, Woesz A, Pilz C, Rumpler M, Fratzl-Zelman N, Roschger P, Stampfl J, Fratzl P. Biomimetic mineral–organic composite scaffolds with controlled internal architecture. J Mater Sci Mater Med. 2005;16:1111.
28. Suh JY, Jang BC, Zhu X, Ong JL, Kim K. Effect of hydrothermally treated anodic oxide films on osteoblast attachment and proliferation. Biomaterials. 2003;24:347.
29. Smiciklas I, Onjia A, Raicevíc S. Factors influencing the removal of divalent cations by hydroxyapatite. J Hazard Mater. 2008;152:876.

30. Tokuda S, Obata A, Kasuga T. Preparation of poly(lactic acid)/siloxane/calcium carbonate composite membranes with antibacterial activity. Acta Biomat. 2009;5:1163.
31. Santos C, Franke RP, Almeida MM, Costa MEV. Nanoscale characterization of hydroxyapatite particles by electron microscopy. Microsc Microanal. 2008;14(supp 3):67.
32. Jaya S, Durance TD, Wang R. Preparation and physical characterization of gelatin-starch/hydroxyapatite porous composite scaffold fabricated using novel microwave energy under vacuum technique. J Composite Materials. 2009;43:1451.
33. Melaiye A, Sun ZH, Hindi K, Milsted A, Ely D, Reneker DH, Tessier CA, Youngs WJ. Silver(I)-imidazole cyclophane gem-diol complexes encapsulated by electrospun tecophilic nanofibers: formation of nanosilver particles and antimicrobial activity. J Am Chem. 2005;127:2285.
34. Chau HH, Jan T, Christina S, Ralf T, Joerg CT. Nanoseparated polymetic networks with multiple antimicrobial properties. Advanced Materials. 2004;16:957.
35. Kuroda K, DeGrado WF. Amphiphilic polymethacrylate derivatives as antimicrobial agents. J Am Chem Soc. 2005;127:4128.